

Numerical Research on Multi-Particle Movements and Nozzle Wear Involved in Abrasive Waterjet Machining

Mingming Du (✉ dumingming@zju.edu.cn)

Zhejiang University <https://orcid.org/0000-0003-4107-0745>

Haijin Wang

Zhejiang University

Huiyue Dong

Zhejiang University

Yingjie Guo

Zhejiang University

Yinglin Ke

Zhejiang University

Research Article

Keywords: Abrasive waterjet cutting, Whole-stage model, Cutting characteristic, Particle velocity and trajectory, Nozzle wear.

Posted Date: June 1st, 2021

DOI: <https://doi.org/10.21203/rs.3.rs-186455/v1>

License:   This work is licensed under a Creative Commons Attribution 4.0 International License.

[Read Full License](#)

Version of Record: A version of this preprint was published at The International Journal of Advanced Manufacturing Technology on August 18th, 2021. See the published version at <https://doi.org/10.1007/s00170-021-07876-9>.

Abstract

Multi-particle velocities and trajectories in abrasive waterjet machining are of great value to understand the particle erosion mechanism involved in the cutting process. In this paper, the whole-stage simulation model is established from the high-pressure water and abrasive particles entering the nozzle to the mixed abrasive jet impacting the workpiece based on the SPH-DEM-FEM method. Comparing the simulation results with the experimental results under different process parameters, the capability of the proposed model is systematically validated. The model is applied to study the mixing and accelerating process of abrasive particles, and the results show that a speed difference is existed between the water and abrasive particles after being ejected from the nozzle. In addition, the nozzle wear pattern is also analyzed carefully. It is discovered that the most serious wear happened at the junction of the mixing chamber and the focusing tube. And the focusing tube wear is uneven and spreads downward.

1. Introduction

Abrasive waterjet machining (AWJM) is a typical high-energy fluid jet machining technology. The abrasive particles are entrained within the high-velocity waterjet and accelerated inside the nozzle head [1]. It offers superior processing performance, such as negligible heat-affected zone, low specific cutting force, and high flexibilities over other conventional (e.g., milling, turning) or non-conventional machining techniques (e.g., electrical discharge machining, laser). Thus, it is being widely and increasingly utilized to machine hard-to-cut materials like engineered ceramics [2], composites [3], and high strength steel [4], for instance. Despite all the advantages mentioned above, there are some challenges in the AWJM fields. The cutting qualities, especially the kerf geometrical characteristics and surface integrities, are susceptible to energetic, kinematic, and constructive parameters, which result in the difficulties of controlling the AWJM process.

Plenty of academics devote themselves to exploring the influence of process parameters on cutting quality. Hashish [5] divided the parameters involved in the AWJM operation into two categories. The first group was related to the AWJM itself, including the hydraulic, abrasive, and mixing parameters. And the second group mainly included kinematic parameters such as standoff distance and traverse speed etc. Wang et al.[6] established empirical models to predict the kerf geometry and surface roughness based on extensive experimental data. Additionally, there were different kinds of intelligent optimization algorithms, such as multi-objective artificial bee colony algorithm [7], extreme learning machine (ELM) [8], and artificial neural networks (ANNs) [9] implanted to achieve a higher quality of AWJM. But a large number of experiments are required to build an accurate optimization model, which is labor-intensive. And some essential outputs like the uniformity of abrasive particles mixed with waterjet inside the nozzle are hard to be acquired by measurements because of the extreme operating conditions.

It is well known that high-fidelity numerical simulations play a critical role in assisting in understanding the complex mechanisms, which could significantly save cost and time. Hence, various numerical strategies are adopted to build the AWJM models to study the flow characteristics inside the nozzle [10–

12] and the high-speed impact erosion mechanism on the target [13–17]. Computational fluid dynamics (CFD) methods were mainly employed to investigate jet flow characteristics. Qiang et al. [10] carried out CFD simulations of three-phase flow to analyze the mixing and accelerating process of the abrasive particles inside the nozzle head. The effects of constructive parameters (i.e., abrasive inlet angle, abrasive inlet position, and focusing tube converging angle) on the nozzle wear were also discussed in detail. The knowledge of the energy distribution across the water jet is one of the most crucial factors affecting the cutting quality. Liu et al. [11] and Wang [12] attempted to establish a CFD model of ultra-high pressure AWJM to study the dynamic characteristics of waterjet outside the nozzle. The results indicated that the waterjet velocities at a given cross-section of the outflow formed a top-hat profile where the velocity at the jet center was higher than the boundaries.

Although CFD based models show the detailed features of the internal and external flow field, it is unable to demonstrate the particle erosion process on the workpiece. Consequently, numerous researches in the literature have concentrated on modeling high-speed particle impact damages on the target using finite element analysis (FEA) [13–15] and smoothed particle hydrodynamics (SPH) [16, 17]. Eltobgy et al. [13] conducted the explicit FEM simulations of the single-particle erosion process at different velocities and impact angles, which was proven to be consistent with the research by Finnie[18] Bitter[19], and Hashish[20]. Furthermore, Anwar et al. [14, 15] extended the simulations into multiple-particle situations. The abrasive particles were presented in non-spherical shapes with sharp cutting edges. Besides, the SPH method is also widely used in modeling AWJM. Wang et al. [16] firstly advocated that the waterjet containing abrasives could be established in SPH particles. Then Dong et al. [17] further modeled abrasive particles into arbitrarily shaped rigid bodies and considered the interaction between fluid and abrasives. However, the above models adopted the simplified motion laws of the internal flow field inside the nozzle head. The velocity distribution at a given cross-section of the jet beam was assumed to be the same. Thus, the previous models are unable to predict the kerf profiles accurately. It is necessary to develop the simulation models of the whole AWJM process which takes both internal and external flow fields into consideration.

To address the requirements, Gong et al. [21] built a numerical model to simulate the whole process stage of AWJM using the coupled ALE-FEM method. The water flow, which had large deformation during processing, was expressed by the arbitrary lagrangian eulerian (ALE) method. The mixture of water and abrasives was achieved by setting a keyword defining the volume fraction of different materials in the initial ALE elements. The lagrangian elements were used for the target. But there were no discrete abrasive particles in the model. The momentum transfer between the abrasives and the waterjet was ignored. Feng et al.[22] attempted to use the coupled SPH-FEM method to establish the whole process model of AWJM. In their study, one abrasive particle in low velocity was accelerated by the high-speed water stream escaped from the fine orifice and eventually impacted the target. The dynamic characteristics of the mixing and acceleration of particles inside the nozzle head were discussed in detail. Nevertheless, there was only one abrasive particle in the model. The contact between abrasive particles was neglected. Besides, the abrasive particles and water flow particles were pre-established in the model, which could not only increase the model size but also limit the simulated cutting depth.

Although there have been some pioneer researchers [21, 22] who put much effort into the whole stage simulations of AWJM, the established models are still far different from the actual processing situations. The complexities, such as the mixing and accelerating process between particles and waterjet, the collisions among particles, and the high-speed particle erosions on the target, etc., have greatly increased the difficulties in modeling. On account of this, the coupled SPH-DEM-FEM modeling strategy is applied to the whole-stage AWJM model. The fluid with extra-large deformation is modeled by the SPH method; the multiple abrasive particles are expressed by the discrete element method (DEM), and the nozzle head and the workpiece are meshed by FEM grids. Besides, a large number of SPH and DEM particles are continuously injected from the inlet, which is much more alike to the actual cutting operations. To evaluate the scalability of the newly developed model for various operating conditions on metal specimens, the dynamic characteristics of the internal flow field, the nozzle wear induced by abrasives, and the impact stress of the target are discussed in detail. In addition, experiments are carried out to verify the correctness of this model.

2. The Basic Theory Of Waterjet Dynamics

2.1. Dynamic characteristics of the flow field inside the nozzle

One of the urgent requirements for AWJM modeling is to have a deep understanding of the jets' erosive efficacy, which is closely related to the momentum exchange from high-speed waterjet to abrasive particles inside the nozzle head. The spatial position and velocity distribution of particles are essential factors in the structural design of the nozzle head and have a significant influence on the cutting quality [23].

(1) The mixing and accelerating process of abrasive particles

During AWJM operations, the high-speed water jet escaped through the sapphire orifice forms negative pressure in the mixing chamber. The abrasive particles flow into the mixing chamber with air, and the mass flow rate is controlled by a step motor in order to feed the abrasives evenly and continuously. Because the diameter of abrasive flow is much larger than the size of jet, only a few abrasives are mixed into the jet directly when the abrasives first come into contact with the waterjet. The rest of the abrasives slide along the chamber wall and gradually merge into the jet after multiple collisions and rebounds in the focusing tube. The abrasive particles are thoroughly mixed and accelerated by the high-pressure water. As a result, a uniform abrasive waterjet is formed in the nozzle head and then impacts the workpiece at high velocity [24, 12]. The close up of the nozzle structure is illustrated in Fig. 1.

(2) Nozzle wear

In the mixing and accelerating process, the abrasive particles continually collide and rub with the inner wall of the nozzle head, resulting in abrasion of the mixing chamber and the focusing tube. The nozzle

wear is one of the main reasons leading to the reduction of processing quality and efficiency. However, due to the powerful destructive force of high-speed abrasive waterjet and the small size of the nozzle structure, nozzle wear is difficult to directly measure. Moreover, the theoretical model adopts many assumptions because of the random collision erosion of abrasive particles, which limits the accuracy of the model. Therefore, the motive of this research is to reveal the laws of nozzle wear from the abrasive particle movements in the focusing tube by simulations. The analysis can also be used to guide the design of the nozzle structure.

Finnie's wear law is used in the developed model of this paper to calculate the abrasive wear on the nozzle wall [25]. In the particle erosion model proposed by Finnie, the wear rate is related to the kinetic energy of the particle impacting on the surface as

$$Q = \begin{cases} \frac{mv^2}{8p} (\sin 2\alpha - 3 \sin^2 \alpha) & \text{if } \tan \alpha < \frac{1}{3} \\ \frac{mv^2}{24p} \cos^2 \alpha & \text{if } \tan \alpha > \frac{1}{3} \end{cases} \quad (1)$$

where Q is the volume of material removed from the surface, m is the particle mass, α is the impact angle, and p is the yield stress of the target material.

2.2. Dynamic characteristics of the external flow field

(1) Waterjet structure

The velocities and convergence of waterjet have significant effects on the characteristics of the kerf, as shown in Fig. 2. The jet beam is divergent, and the effective width of the jet, which represents the jet cutting ability, is smaller than the jet width. Besides, particle velocities at any cross-section of jet change from zero at the jet boundary to the maximum value of the jet center, which is corresponded to the energy distribution of the jet. Yanaida et al. [26] proposed an empirical model to calculate the spreading radius of waterjet as

$$R = \frac{d_n}{2} + Cgh \quad (2)$$

where R defines the waterjet spreading radius in the transition zone, d_n is the orifice diameter, C is the spreading coefficient, and h is the standoff distance.

(2) The impact force of abrasive waterjet

Since the waterjet machining operations are usually performed by the waterjet in the transition zone, the distribution of pressure and velocity in the transition zone has been a hotspot in the field of AWJM. Some theoretical models have been developed to explore the impact energy of the waterjet. Momber et al. [27] established the integration of the impact force overtime according to the impact momentum relationship of the jet and obtained the relationship between the jet impact force and the jet velocity as

$$F = \frac{\pi \rho_w d^2}{8} v^2 \quad (3)$$

where F is the impact force; v is the waterjet velocity; d is the effective diameter of the jet beam impacting the workpiece; ρ_w is the density of water.

3. Numerical Modeling Method

The simulation of AWJM is a challenging task, in which the problems of fluid-structure interactions and particle erosion are involved. In addition, there are a variety of materials with different properties, such as continuous water flow, discrete abrasives, and metal included in the process. Due to the multi-physics, multi-scale, and multi-stage issues of the AWJM process, an abrasive water jet impact model is established based on the coupled SPH-DEM-FEM method. The method was elaborated in the previous paper [28].

(1) Waterjet model

The waterjet, which suffers large deformation in AWJM, is based on the SPH method. The NULL material model, coupled with the MURNAGHAN equation of state, is used to describe the behavior of water [25]. The material parameters required in the waterjet model are acquired from the research of Wang [29]. Additionally, the waterjet is injected from the orifice in this model, which is just like the realistic AWJM operations, and the enhanced fluid formulation [30] is recommended to model the fluid behavior. Moreover, the initial velocity of water is calculated by Bernoulli's law considering compressibility [31].

(2) Abrasive particle flow model

In this model, DEM formulations are used to simulate the abrasive particles. The rigid material model is selected for the abrasive particle material owing to the high hardness of garnet. The parameters of the particle material are obtained from Feng [22]. Besides, DEM spheres could act like non-spherical particles by setting the discrete element control and contact parameters [28].

(3) Nozzle model

According to the practical application and economic principle, a simplified nozzle body model is shown in Fig. 3. The nozzle body is modeled by shell elements. The parameters of the geometric model used in this study are shown in Table 1. Besides, the elastoplastic material model is adopted in the finite element structure. The generally used material of the nozzle is tungsten carbide (WC) with a mass density of 15.63g/cm^3 , Poisson's ratio 0.31, and Young's modulus 550 GPa.

Table 1
Geometric parameters of the AWJM nozzle

Value	Parameters (mm)
Focusing tube diameter d_1	1.02
Mixing chamber diameter d_2	5
Orifice diameter d_3	0.33
Particle inlet diameter d_4	3
Focusing tube length L_1	76.2
Mixing chamber length L_2	10
Particle inlet angular $\theta(^{\circ})$	45
Converging part angular $\alpha(^{\circ})$	60

(4) Workpiece model

As for the high strain rates of the impacted target, the Johnson-Cook material model, coupled with the GRUNEISEN equation-of-state, is utilized in the present model. The required material parameters of C45 steel are acquired from the previous work [28]. Besides, the dimensions of the workpiece are 10×10×2 mm with 102,400 eight-node solid elements for the structural analysis of the target. The non-reflection boundary condition is set on the surrounding surface of the target. The whole model is illustrated in Fig. 4.

4. Experiments Design

The experiments to verify the authenticity of the simulation model were conducted on a 6-axis robot (Fanuc M20IA) equipped with the end effector (KMT waterjet cutting head). The ultra-high pressure pump utilized in the tests was KMT SL-VI 50, with a maximum pressure of 413.7 MPa (60,000 psi). Besides, the geometric parameters of the nozzle head were the same as the model parameters, which are listed in Table 1. The workpiece used in the test was a 200 mm×100 mm×20 mm rectangular slab made in the C45 steel material. The almandine garnet sand mesh 80 was employed as the abrasive particle.

One of the advantages of the whole process model of the AWJM is that it can study the influence of the standoff distance on the geometric characteristics of the cutting kerf. Therefore, the experiments were designed to compare the error of the kerf top width and cut depth between the simulation and the test results under the influence of various parameters, including traverse speed, water pressure, abrasive mass flow rate, and standoff distance. The experimental parameters are shown in Table 2.

Table 2
Operation parameters in the AWJM experiments

Parameters	Description
Water pressure	200, 240, 280, 320, 360 MPa;
Standoff distance	2, 3,4,5,6 mm;
Traverse speed	80, 120,160,200,240 mm/min;
Abrasive mass flow rate	0.045,0.090,0.135,0.180 kg/min;
Jet impact angle	90°

After the AWJ cutting tests were completed, the Keyence 3D contour scanner (LJ-X8060) was used to measure the kerf profiles. The measured length was 60mm along the traverse speed direction. In order to verify the results of the simulation model, the average profile was taken as the measurement result. The experimental setup and measurement process are illustrated in Fig. 5.

5. Results And Discussion

5.1 Validation of the whole-stage model of AWJM

The explanation of the simulation process for the whole-stage AWJM model is illustrated in Fig. 6. In Fig. 6 (a), the high-speed waterjet is injected from the orifice and interacts with the low-speed abrasive flow in the mixing chamber. Figure 6 (b) represents the mixing and accelerating progress of abrasives and waterjet in the focusing tube. Figure 6 (c) shows the mixed jet flowing out of the focusing tube and impacting the workpiece surface. Figure 6 (d) demonstrates the final state of the target after the jet impact. Besides, the geometric profile of the kerf in Fig. 6 (d) is used to compare with the contour data obtained from experiments.

Because the velocity distribution of waterjet has been taken into account in the whole-stage model, it can be applied to study the influence of the standoff distance on cutting quality. According to Fig. 7 (a), the standoff distance has little influence on the cutting depth of kerf. It appears that the kerf depth is sensitive to the variables related to jet energy, such as traverse speed, abrasive flow rate, and so on [32]. On the contrary, the standoff distance has a much more significant effect on the geometric characteristics of the kerf, especially the top width of the kerf. It is shown from Fig. 7 (b) that the top width increases as the target distance increases which is consistent with the experimental data. This trend can be attributed to the fact that the effective diameter of the waterjet increases when the jet exits the nozzle outlet. Consequently, a wider inlet kerf is cut as the standoff distance increases.

What's more, the simulation results of the whole-stage model are compared with the experimental results and the external flow field model results [28] in terms of abrasive mass flow rate, water pressure, and traverse speed as shown in Fig. 8 to Fig. 10. The variation of the cutting depth and the top cutting width

with abrasive mass flow rate is illustrated in Fig. 8. When the abrasive mass flow is increased from 0.045 kg/min to 0.180 kg/min, and the water pressure is kept at 360MPa, the traverse speed is 80 mm/min, the depth of cut changes from 17.896 to 19.198 mm. The kerf width changes from 1.462 to 1.563mm. The simulation results of the whole-stage model are in good agreement with the experimental data.

Figure 9 shows the variation of cutting depth and top cutting width in AWJM with jet pressure. When the traverse speed is 80 mm/min, the abrasive mass flow is 0.12 kg/min, and the jet pressure increases from 200MPa to 360MPa, the cutting depth is increased from 15.198mm to 19.198mm. The cutting width is increased from 1.410mm to 1.652mm. Figure 10. demonstrates the change of cutting depth and top cutting width with traverse speed. When the rate is increased from 80mm/min to 240mm/min, the cutting depth is decreased from 19.198mm to 2.719mm, and the cutting width is decreased from 1.556mm to 1.226mm at the water pressure 360MPa.

In summary, the predicted results of the whole-stage model are consistent with the experimental results with an error of 20% in predicting cut depth and an error of 30% in predicting kerf width, respectively. It can be seen that the prediction accuracy of the kerf top width of the whole stage model is significantly improved, but the predicted kerf depth is shallower than that of the external flow model. This is because that the abrasive particle velocity in the whole process model is calculated through the mixing acceleration process in the nozzle. But in the external flow field model, the waterjet structure is uniform, and the velocity difference between the abrasive particles and the water flow is ignored. Therefore, it can be concluded that the whole-stage model has more advantages in predicting the contour of the kerfs.

The model is further verified by the effective pressure magnitude of the waterjet impacting the workpiece surface. When the high-pressure waterjet is injected into the nozzle at 600m/s, the hydraulic shock pressure predicted by the whole-process simulation model is shown in Fig. 11. The maximum effective stress is 170.115MPa. And the jet impact force is illustrated in Fig. 11 (b). It can be seen that the resultant force oscillates around 50N, while the maximum impact force is 86.4 N and the minimum impact force is 14.6 N. Besides, the impact pressure can be calculated as 179.676MPa by Eq. (3) when the nozzle exit diameter is assumed as the effective diameter of the jet beam. It proves that the whole process model established in this paper can effectively calculate the impact pressure of the waterjet.

5.2 The mixing and accelerating process of abrasive particles

The whole stage simulation model of AWJM is established in this paper to study the mixing and acceleration process of abrasive particles with waterjet in the nozzle, as shown in Fig. 12 (a). When the jet beam is ejected from the orifice at an initial velocity of 600 m/s, the abrasive particles are sucked into the mixing chamber at low speed. Because the diameter of the jet beam is much smaller than the abrasive flow, the abrasive flow is dispersed into two parts by the impact of the jet beam, and the part of the abrasive flow hit by the high-speed jet is reflected on one side of the mixing chamber wall which is denoted by part "a" in Fig. 12 (b). Its speed is increased rapidly to 300m/s and dropped to 164m/s after

clashing with the wall. Subsequently, the particles enter into the focusing tube and are fully mixed with the waterjet. The speed gradually accelerated to approximately the speed of the waterjet as 542m/s, as exhibited in Fig. 13 (a). The other particles do not strike with the high-speed jet in the mixing chamber as part “b” in Fig. 12 (b). And its speed change is shown in Fig. 13 (b). After entering the mixing chamber, these particles collide with the mixing chamber wall directly and slide down the wall. Finally, the particles also go into the focusing tube and are accelerated to a speed of 561m/s.

The evolution of waterjet velocity is demonstrated in Fig. 13 (c). The waterjet is injected into the mixing chamber at the speed of 600 m/s and completely mixed with the abrasive particles in the focusing tube. It can also be observed that the speed of the water flow in the nozzle is reduced. This is accounted for the fact that the energy exchange process steals some energy from the waterjet, thereby reducing the jet speed to 580m/s. But the exit velocities of the waterjet and the particle ejected from the nozzle are not the same. The velocity of the waterjet is slightly higher than the speed of abrasive particles. When the waterjet impacts the workpiece, the speed drops rapidly from 580m/s to 26.4m/s. This is consistent with the actual machining situation where the water and abrasive particles are splashed after cutting the target.

5.3 Nozzle wear

The numerical modeling method provides an opportunity to present the spatial distribution of abrasive particles in the waterjet plume, which is more accurate for studying waterjet structure and nozzle wear. Figure 14 shows the trajectory of water flow particles and abrasive particles. It can be seen from Fig. 14 (a) that the trajectory of water flows gradually diverges. In addition, the abrasive particles enter the mixing tube after colliding with the wall surface in the mixing chamber, and the water particles and abrasive particles are gradually mixed evenly during the continuous collision with the focusing tube wall, and finally ejected from the nozzle as illustrated in Fig. 14 (b).

The particle trajectories are closely related to the pattern of nozzle wear which are shown in Fig. 15. The Finnie's wear law is used in the nozzle wear study as mentioned in Sect. 2.1. It is observed that the wear mainly occurs at the junction of the mixing chamber and the focusing tube, where the high-speed jet entrains abrasive particles into the focusing tube. The wear of the focusing tube is uneven and has a tendency to meander and spread downward. Its essence is related to the continuous collision and advancement of abrasive particles against the tube wall as the particle trajectory is shown in Fig. 14. The nozzle wear is consistent with the actual machining situation, as pointed out by Percec et al[33].

6. Conclusions

In this paper, the SPH-DEM-FEM method is adopted to establish the AWJM simulation model of the whole-stage process from the jet beam and the abrasive stream being injected into the nozzle to mixed abrasive water jet impacting the workpiece surface. The authenticity of the simulation model is verified

by comparing it with the experiments. According to the simulation results, the following conclusions can be obtained:

(1) The velocity distribution of the waterjet has been taken into account to predict the cutting depth and kerf width under different parameters. The results prove that the whole-stage model has greatly improved the prediction accuracy of the kerf width.

(2) The model also conducts a deeper study on the mixing and accelerating process of abrasive particles. It is found that the exit velocity of the waterjet is slightly higher than the velocity of the abrasive particles.

(3) The area with the most severe nozzle wear is discovered at the junction between the mixing chamber and the focusing tube. The abrasion of the focusing tube shows a meander and downward trend.

7. Declarations

Competing Interests: The authors declare that they have no conflict of interest.

Ethical Approval: Not applicable

Consent to Participate: Not applicable

Consent to Publish: Not applicable

Availability of data and materials: Available if requested

Authors Contributions

Mingming Du established the simulation model, designed the experiments, and completed the original draft of the research. Haijin Wang helped the experiments and supplied critical revisions. Huiyue Dong is the project leader and provided crucial suggestions. Yingjie Guo offered key paper revisions to the article. Yinglin Ke participated in the paper revision.

Funding

This work was supported by the National Natural Science Foundation of China (No. 51805476 and No. 91748204) and Science Fund for Creative Research Groups of National Natural Science Foundation of China [No.51821093].

8. References

1. Axinte DA, Karpuschewski B, Kong MC, Beaucamp AT, Anwar S, Miller D, Petzel M (2014) High Energy Fluid Jet Machining (HEFJet-Mach): From scientific and technological advances to niche industrial applications. *CIRP Annals* 63 (2):751-771. doi:10.1016/j.cirp.2014.05.001

2. Srinivasu DS, Axinte DA, Shipway PH, Folkes J (2009) Influence of kinematic operating parameters on kerf geometry in abrasive waterjet machining of silicon carbide ceramics. *International Journal of Machine Tools and Manufacture* 49 (14):1077-1088. doi:10.1016/j.ijmachtools.2009.07.007
3. Schwartzentruher J, Spelt JK, Papini M (2018) Modelling of delamination due to hydraulic shock when piercing anisotropic carbon-fiber laminates using an abrasive waterjet. *International Journal of Machine Tools and Manufacture* 132:81-95. doi:10.1016/j.ijmachtools.2018.05.001
4. Tabatchikova TI, Tereshchenko NA, Yakovleva IL, Gudnev NZ (2018) Structure of near-surface layer of high-strength steel subjected to abrasive waterjet cutting. *Physics of Metals and Metallography* 119 (9):871-879. doi:10.1134/s0031918x18090107
5. Hashish M (1991) Optimization factors in abrasive-waterjet machining. *Journal of Engineering for industry* 113 (1):29-37
6. Wang J, Wong WCK (1999) A study of abrasive waterjet cutting of metallic coated sheet steels. *International Journal of Machine Tools & Manufacture* 39 (6):855-870
7. Pawar PJ, Vidhate US, Khalkar MY (2018) Improving the quality characteristics of abrasive water jet machining of marble material using multi-objective artificial bee colony algorithm. *Journal of Computational Design and Engineering* 5 (3):319-328. doi:10.1016/j.jcde.2017.12.002
8. Čojbašić Ž, Petković D, Shamshirband S, Tong CW, Ch S, Janković P, Dučić N, Baralić J (2016) Surface roughness prediction by extreme learning machine constructed with abrasive water jet. *Precision Engineering* 43:86-92. doi:10.1016/j.precisioneng.2015.06.013
9. Çaydaş U, Haşçalık A (2008) A study on surface roughness in abrasive waterjet machining process using artificial neural networks and regression analysis method. *Journal of Materials Processing Technology* 202 (1):574-582. doi:https://doi.org/10.1016/j.jmatprotec.2007.10.024
10. Qiang Z, Wu M, Miao X, Sawhney R (2018) CFD research on particle movement and nozzle wear in the abrasive water jet cutting head. *The International Journal of Advanced Manufacturing Technology* 95 (9-12):4091-4100. doi:10.1007/s00170-017-1504-6
11. Liu H, Wang J, Kelson N, Brown RJ (2004) A study of abrasive waterjet characteristics by CFD simulation. *Journal of Materials Processing Technology* 153-154:488-493. doi:https://doi.org/10.1016/j.jmatprotec.2004.04.037
12. Wang J (2009) Particle velocity models for ultra-high pressure abrasive waterjets. *Journal of Materials Processing Technology* 209 (9):4573-4577. doi:10.1016/j.jmatprotec.2008.10.021
13. Eltobgy MS, Ng E, Elbestawi MA (2005) Finite element modeling of erosive wear. *International Journal of Machine Tools and Manufacture* 45 (11):1337-1346. doi:10.1016/j.ijmachtools.2005.01.007
14. Anwar S, Axinte DA, Becker AA (2013) Finite element modelling of abrasive waterjet milled footprints. *Journal of Materials Processing Technology* 213 (2):180-193. doi:https://doi.org/10.1016/j.jmatprotec.2012.09.006
15. Anwar S, Axinte DA, Becker AA (2013) Finite element modelling of overlapping abrasive waterjet milled footprints. *Wear* 303 (1-2):426-436. doi:10.1016/j.wear.2013.03.018

16. Jianming W, Na G, Wenjun G (2010) Abrasive waterjet machining simulation by SPH method. *The International Journal of Advanced Manufacturing Technology* 50 (1-4):227-234.
doi:10.1007/s00170-010-2521-x
17. Dong X, Li Z, Jiang C, Liu Y (2019) Smoothed particle hydrodynamics (SPH) simulation of impinging jet flows containing abrasive rigid bodies. *Computational Particle Mechanics*:1-23
18. Finnie I (1967) Erosion of metals by solid particles. *Journal of Materials* 2:682
19. Bitter JGA (1963) A study of erosion phenomena part I. *Wear* 6 (1):5-21.
doi:https://doi.org/10.1016/0043-1648(63)90003-6
20. Hashish M (1989) A Model for Abrasive-Waterjet (AWJ) Machining. *Journal of Engineering Materials and Technology* 111
21. Wenjun G, Jianming W, Na G (2010) Numerical simulation for abrasive water jet machining based on ALE algorithm. *The International Journal of Advanced Manufacturing Technology* 53 (1-4):247-253.
doi:10.1007/s00170-010-2836-7
22. Feng Y, Jianming W, Feihong L (2011) Numerical simulation of single particle acceleration process by SPH coupled FEM for abrasive waterjet cutting. *The International Journal of Advanced Manufacturing Technology* 59 (1-4):193-200. doi:10.1007/s00170-011-3495-z
23. Haghbin N, Khakpour A, Schwartzentruber J, Papini M (2019) Measurement of abrasive particle velocity and size distribution in high pressure abrasive slurry and water micro-jets using a modified dual disc anemometer. *Journal of Materials Processing Technology* 263:164-175.
doi:10.1016/j.jmatprotec.2018.08.014
24. Momber AW, Kovacevic R (2012) Principles of abrasive water jet machining. Springer Science & Business Media,
25. LSTC (2019) LS-DYNA keyword user's manual, vol I. Livemore Software Technology Corporation, California
26. Yanaida K, Ohashi SA Flow characteristics of water jets in air. In: Proceedings of the 5th International Symposium on Jet Cutting Technology, United Kingdom (GBR), 1980. pp 33-44
27. Momber A, Kovacevic R (1995) Energy dissipative processes in high speed water-solid particle erosion. In Proceedings of the ASME Heat Transfer and Fluids Engineering Division. American Society of Mechanical Engineers, New York
28. Du M, Wang H, Dong H, Guo Y, Ke Y (2020) Numerical research on kerf characteristics of abrasive waterjet machining based on the SPH-DEM-FEM approach. *The International Journal of Advanced Manufacturing Technology*. doi:10.1007/s00170-020-06340-4
29. Wang F, Wang R, Zhou W, Chen G (2017) Numerical simulation and experimental verification of the rock damage field under particle water jet impacting. *International Journal of Impact Engineering* 102:169-179. doi:10.1016/j.ijimpeng.2016.12.019
30. Yreux E (2018) Fluid flow modeling with SPH in LS-DYNA. Paper presented at the 15th International LS-DYNA Conference, Detroit,

31. Hashish M (2015) WaterJet Machining Process. In: Nee AYC (ed) Handbook of Manufacturing Engineering and Technology. Springer London, London, pp 1651-1686. doi:10.1007/978-1-4471-4670-4_75
32. Yu Y, Sun T, Yuan Y, Gao H, Wang X (2020) Experimental investigation into the effect of abrasive process parameters on the cutting performance for abrasive waterjet technology: a case study. The International Journal of Advanced Manufacturing Technology 107 (5-6):2757-2765. doi:10.1007/s00170-020-05183-3
33. Perc A, Pude F, Grigoryev A, Kaufeld M, Wegener K (2019) A study of wear on focusing tubes exposed to corundum-based abrasives in the waterjet cutting process. The International Journal of Advanced Manufacturing Technology. doi:10.1007/s00170-019-03971-0

Figures

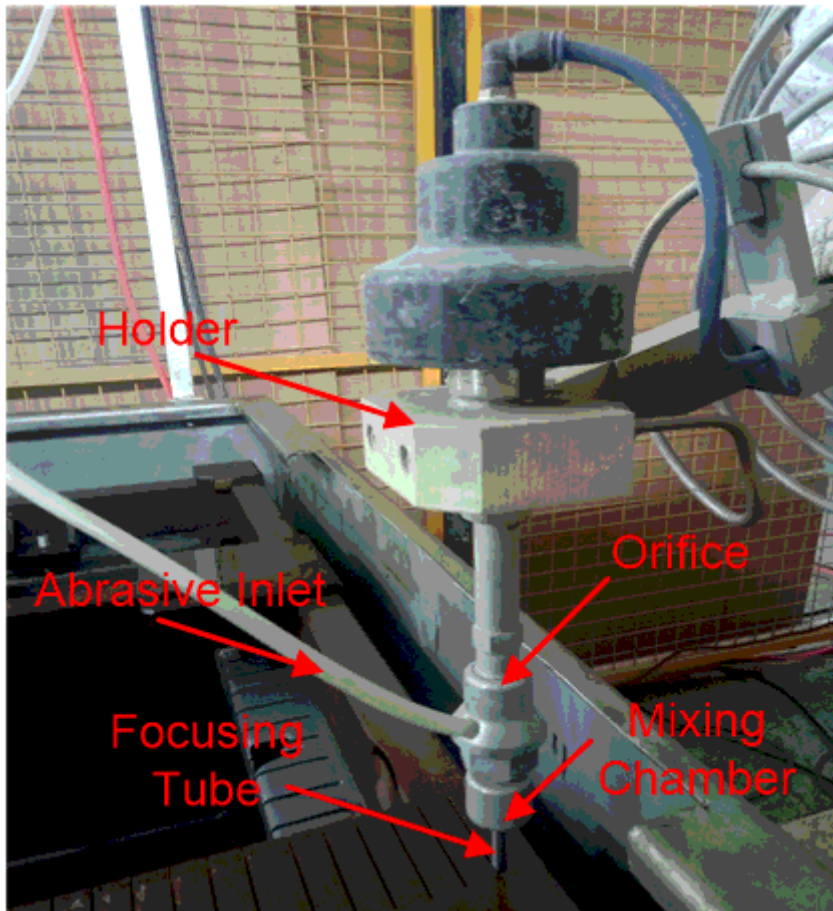


Figure 1

Close-up of the abrasive waterjet nozzle structure

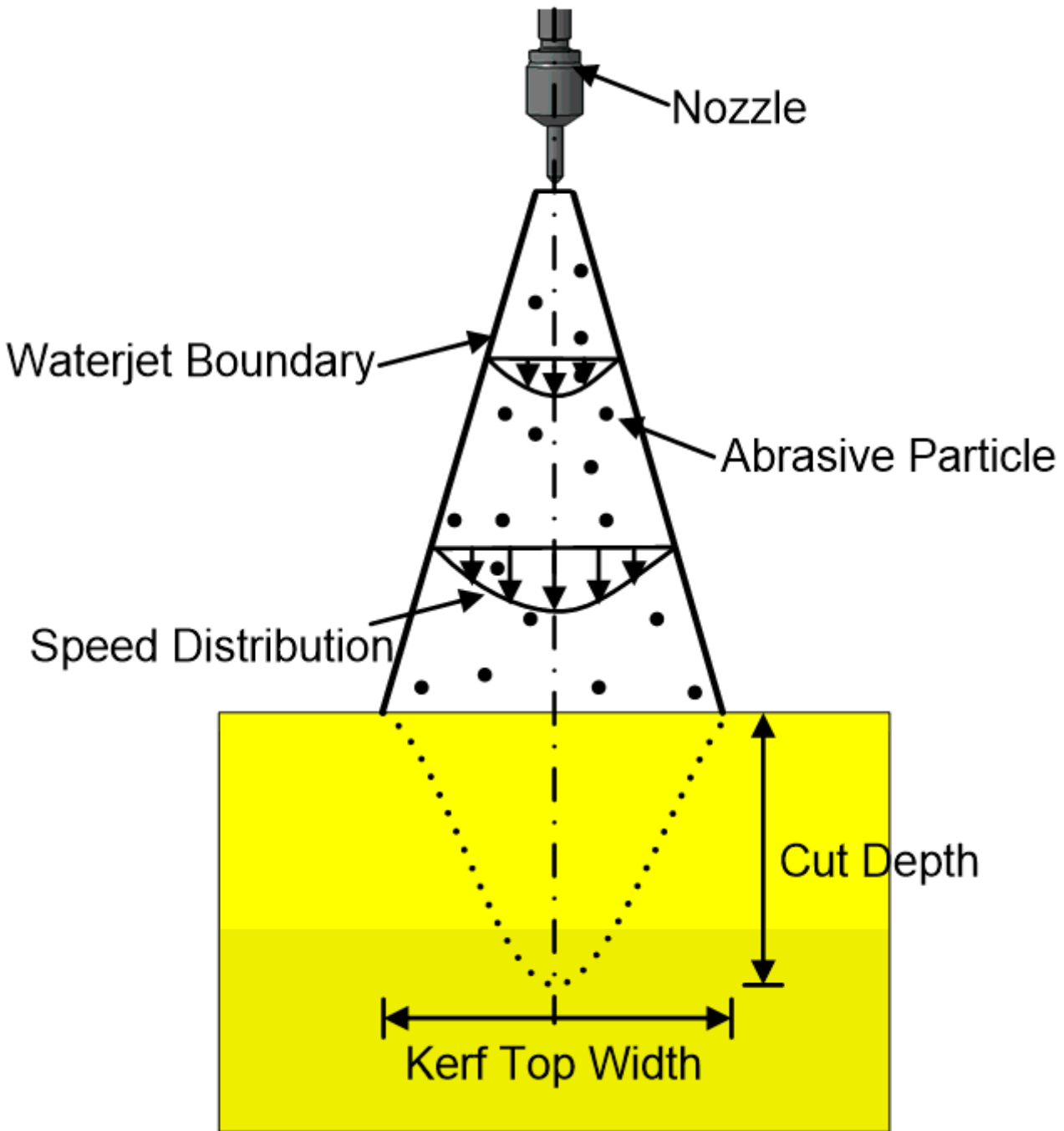


Figure 2

Schematic diagram of the abrasive water jet structure.

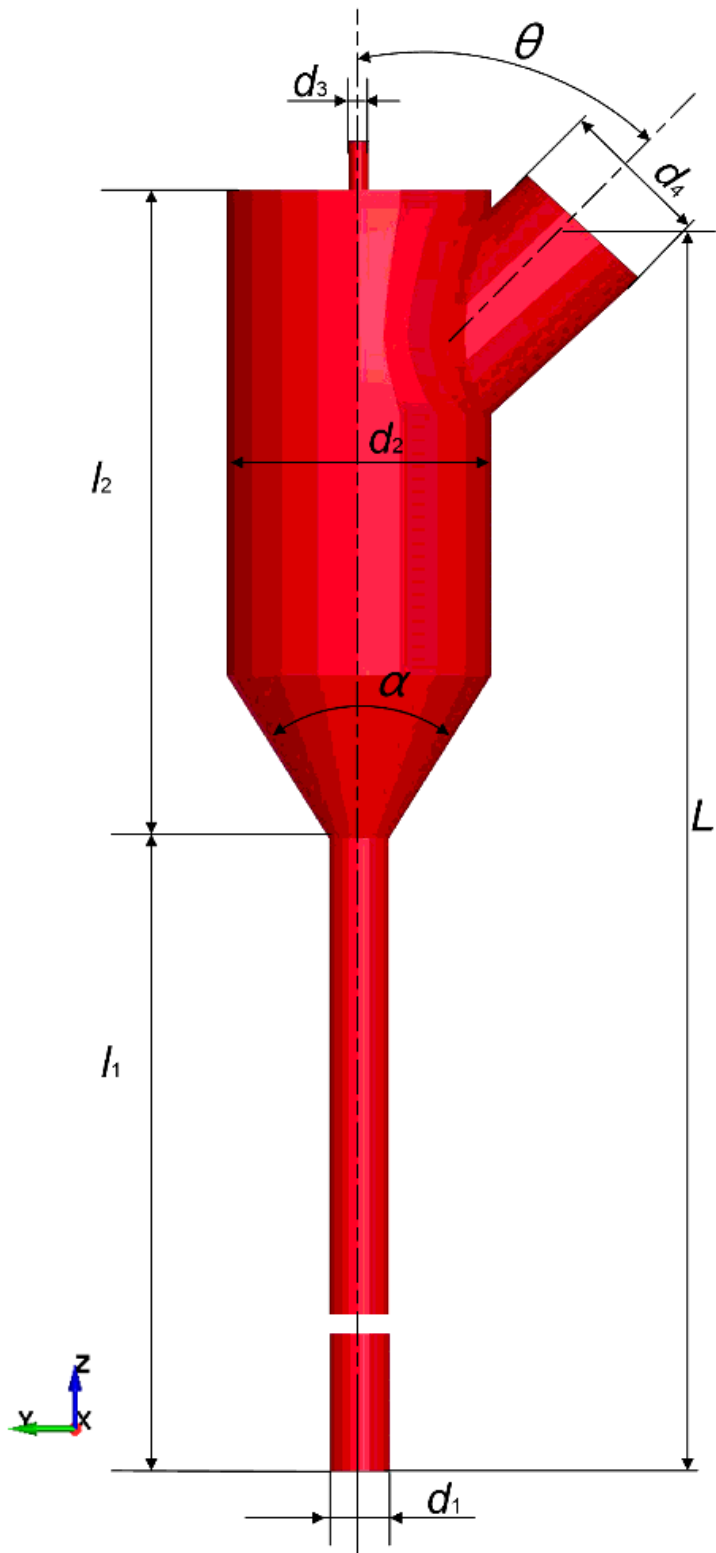


Figure 3

Geometric model of the AWJM nozzle

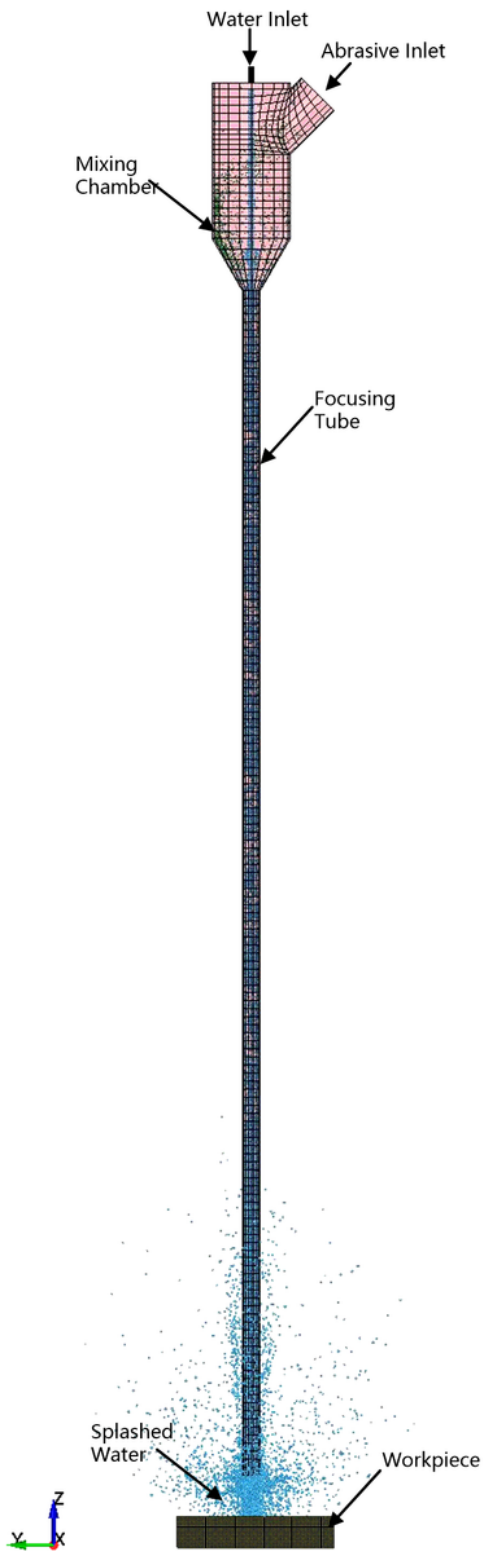


Figure 4

The whole-stage simulation model of abrasive waterjet

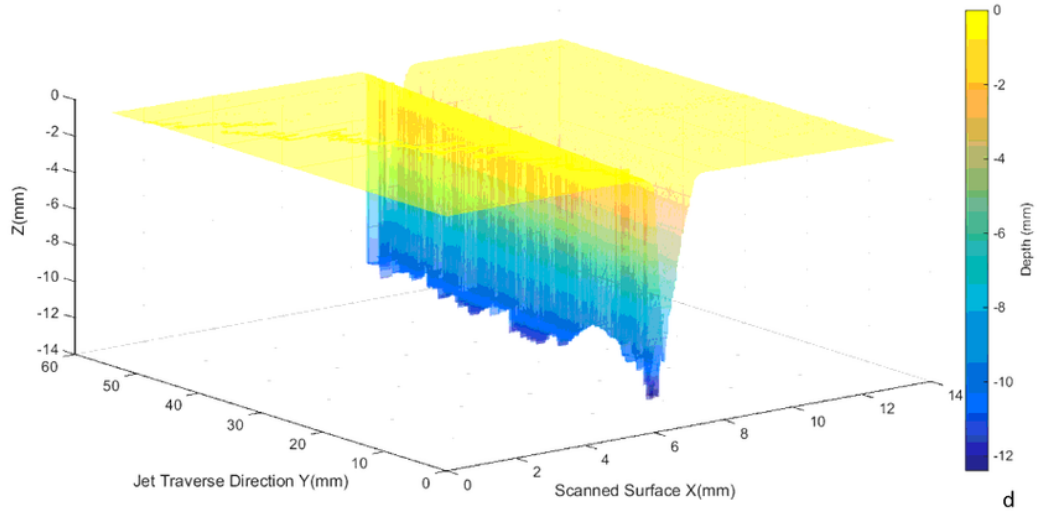


Figure 5

Measurement process for the AWJM experiments. (a) experimental setup. (b) cutting workpiece. (c) measuring instruments. (d) scanned surface.

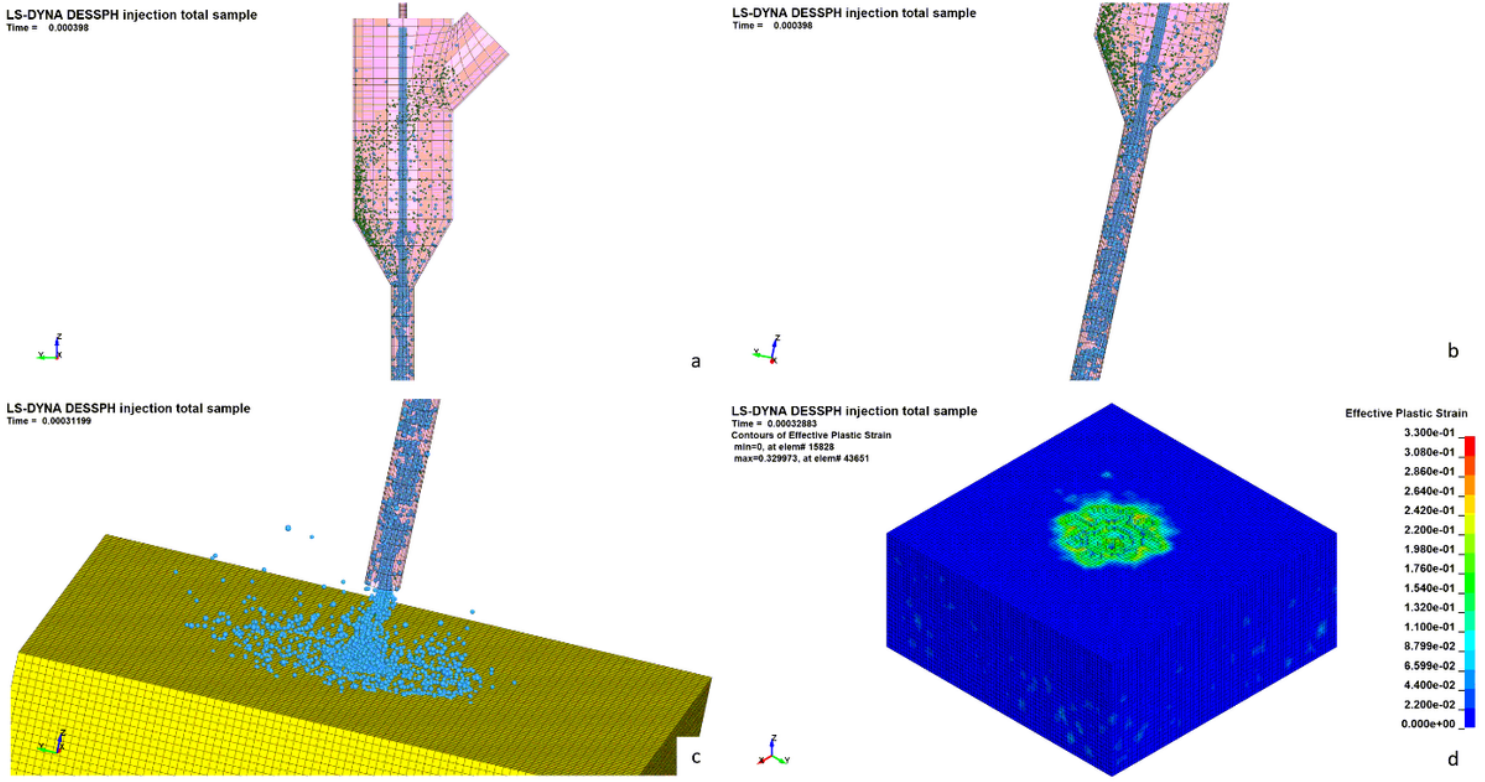


Figure 6

Stages of the simulation process for the whole-stage AWJM model.

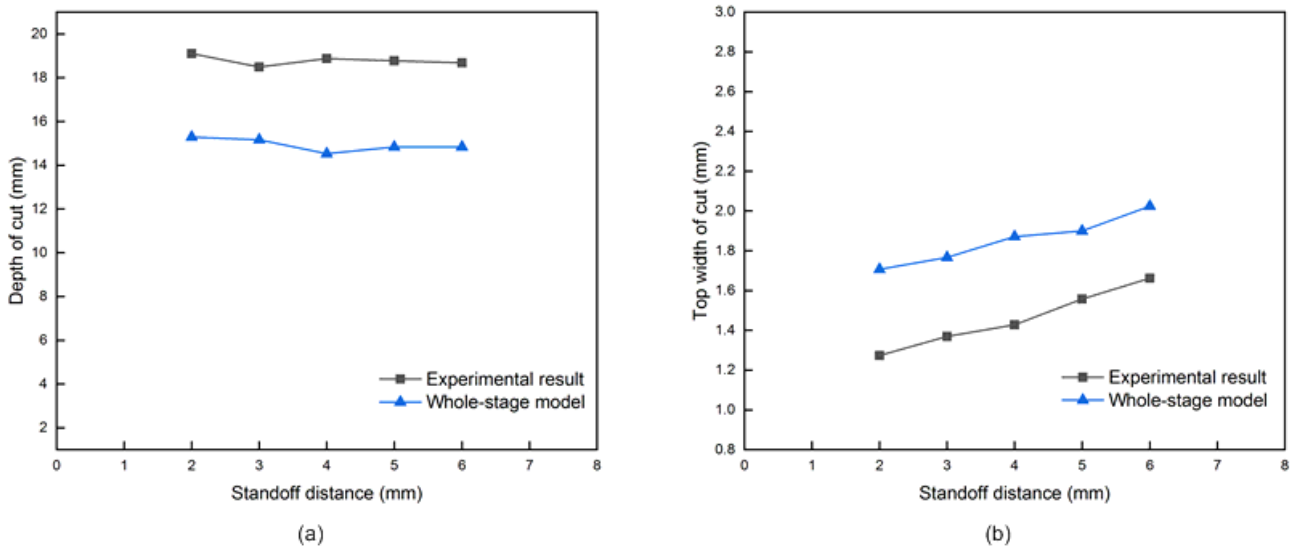
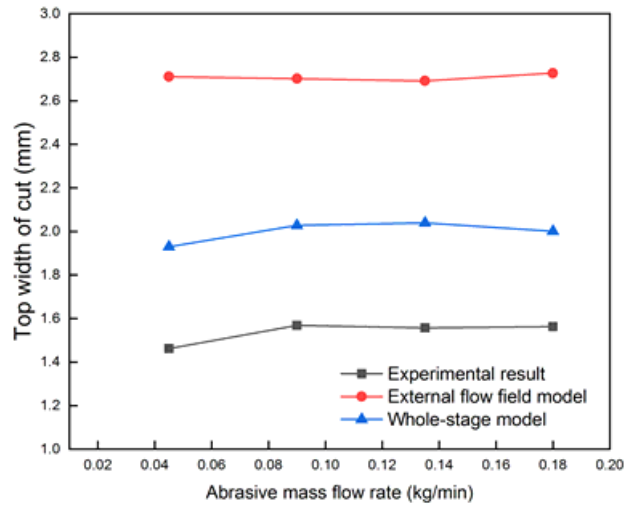
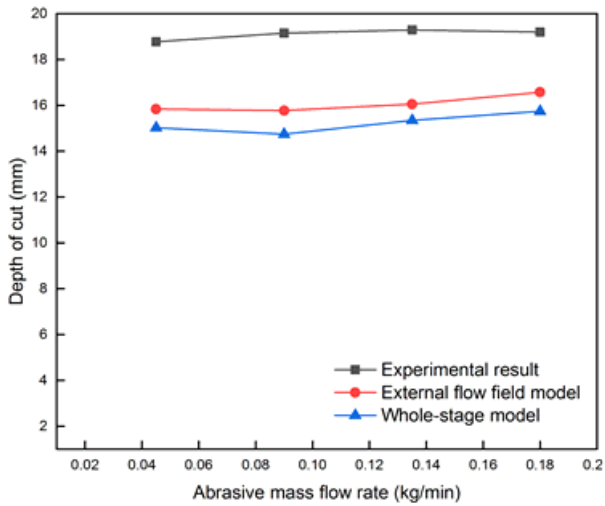


Figure 7

Experimental and simulation results of cutting depth and width under different standoff distance

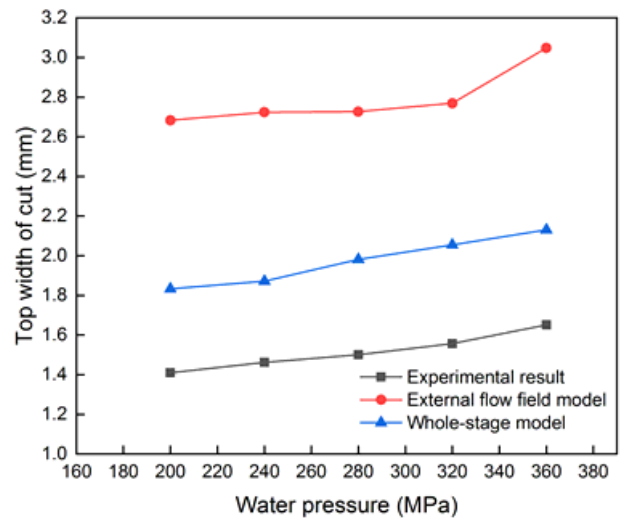
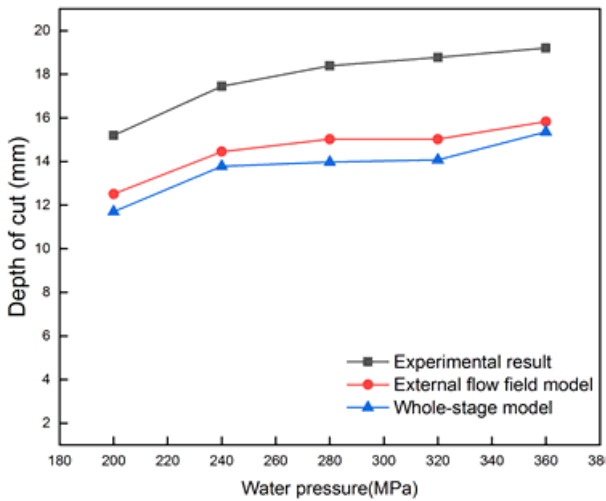


(a)

(b)

Figure 8

Experimental and simulation results of cutting depth and width under different abrasive mass flow rate.

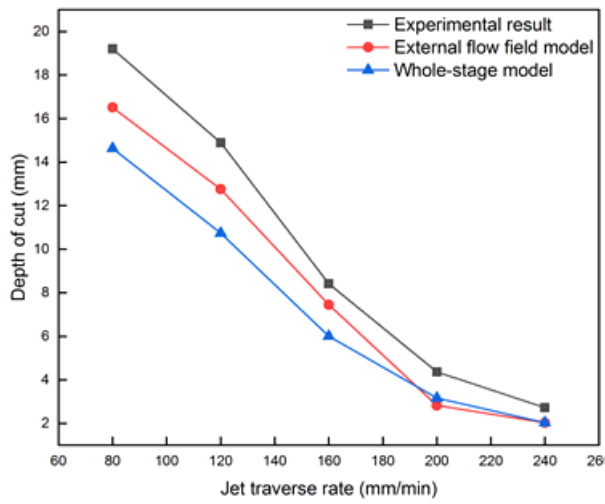


(a)

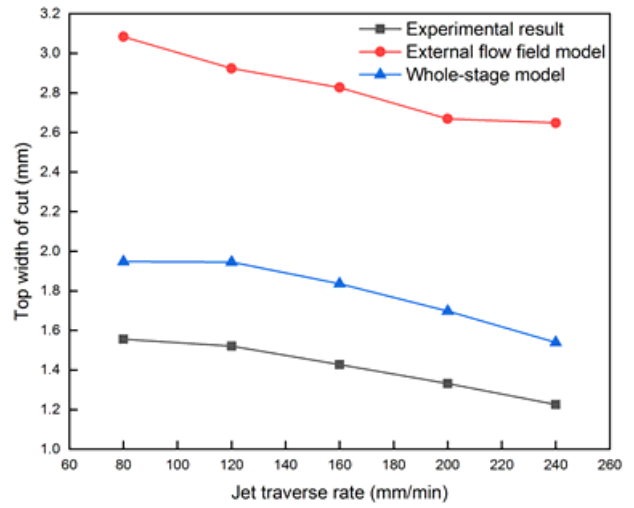
(b)

Figure 9

Experimental and simulation results of cutting depth and width under different water pressure.



(a)



(b)

Figure 10

Experimental and simulation results of cutting depth and width under different traverse rate.

LS-DYNA DESSPH injection total sample

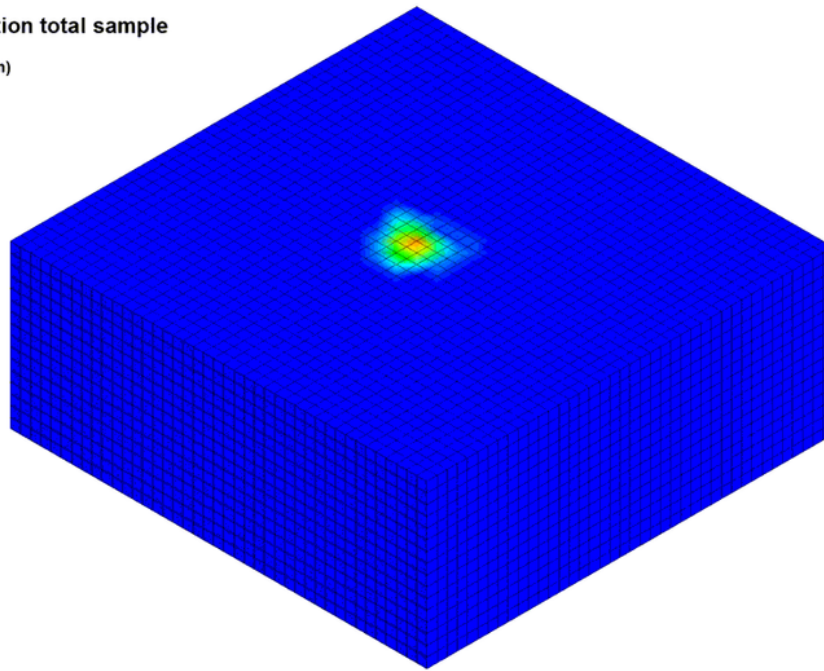
Time = 0.00058598

Contours of Effective Stress (v-m)

max IP. value

min=0.153582, at elem# 18511

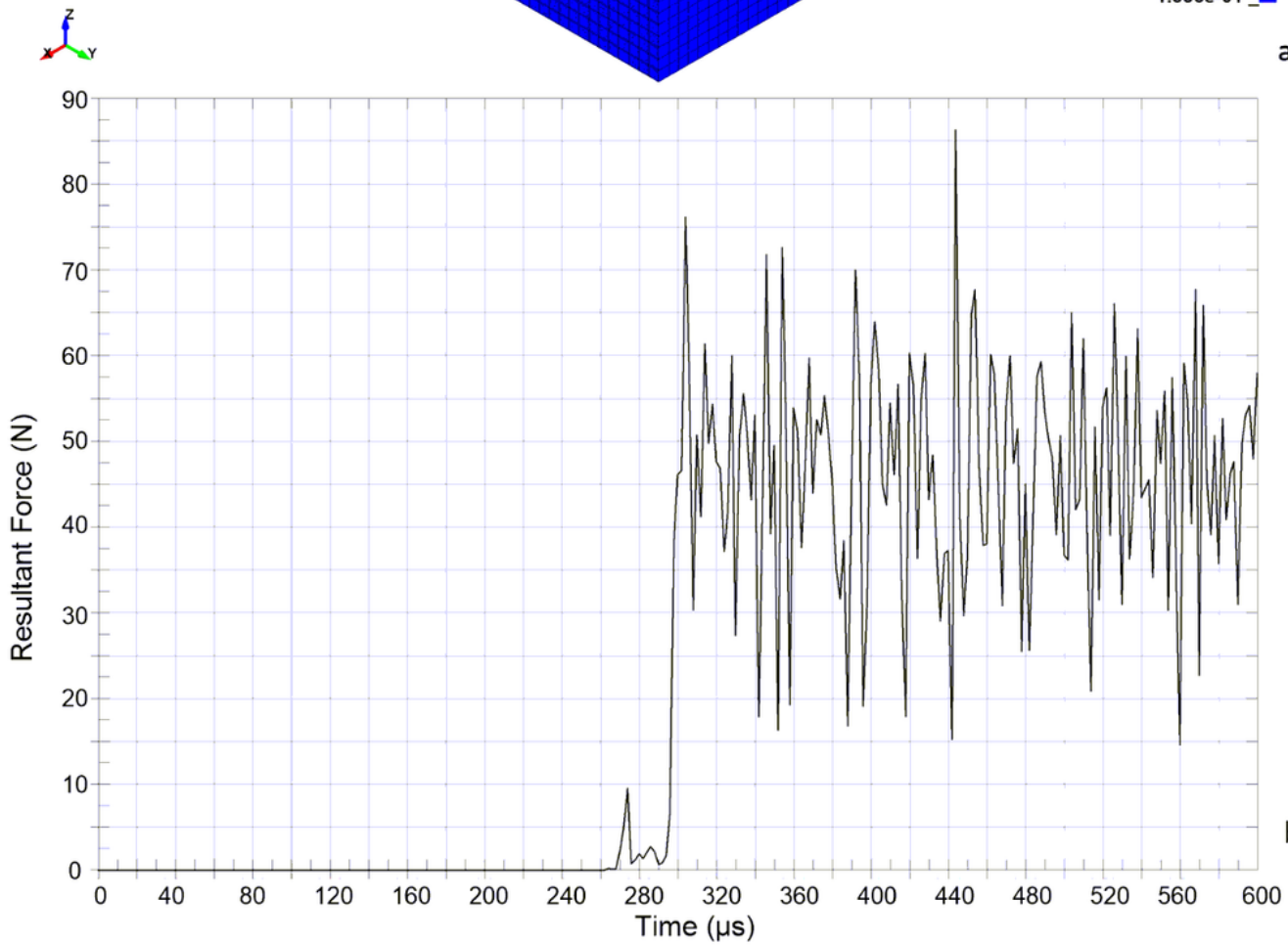
max=170.115, at elem# 43990



Effective Stress (v-m)



a



b

Figure 11

Simulation results of the AWJM effective pressure and resultant force on the workpiece.

LS-DYNA DESSPH injection total sample

Time = 0.00031799
Contours of Resultant Velocity
min=0, at node# 2763
max=638349, at node# 139973



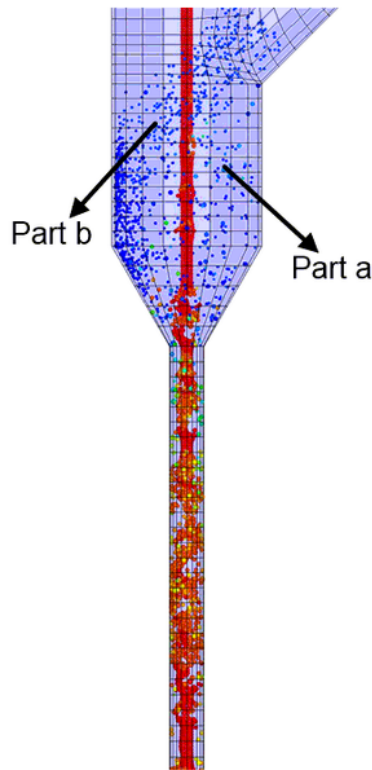
Resultant Velocity



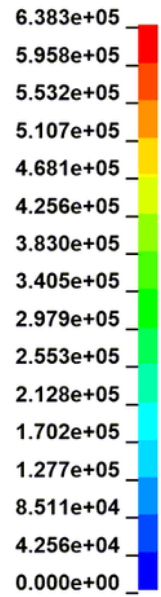
a

LS-DYNA DESSPH injection total sample

Time = 0.00031799
Contours of Resultant Velocity
min=0, at node# 2763
max=638349, at node# 139973



Resultant Velocity



b

Figure 12

The mixing and accelerating process of abrasive particles in the nozzle

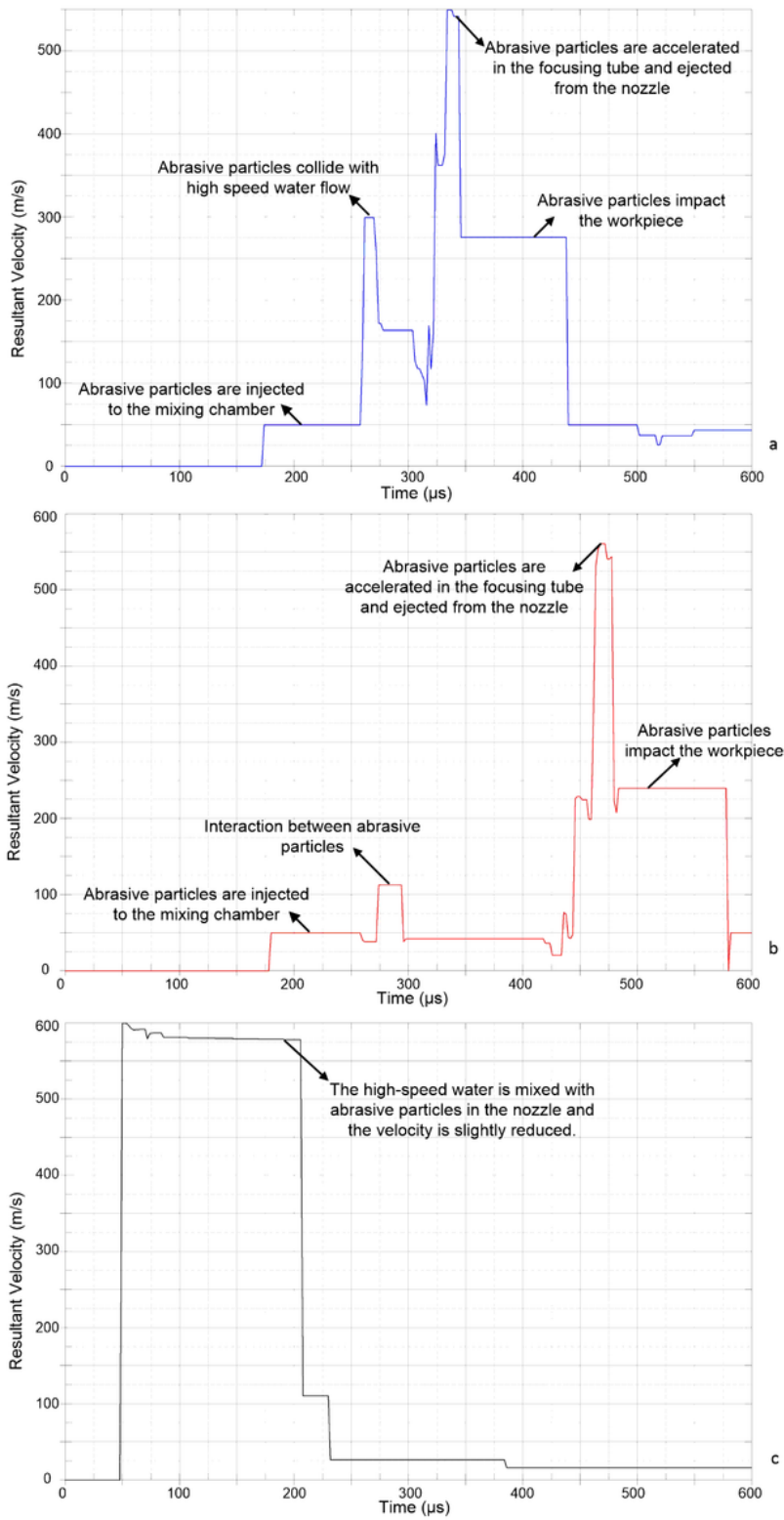
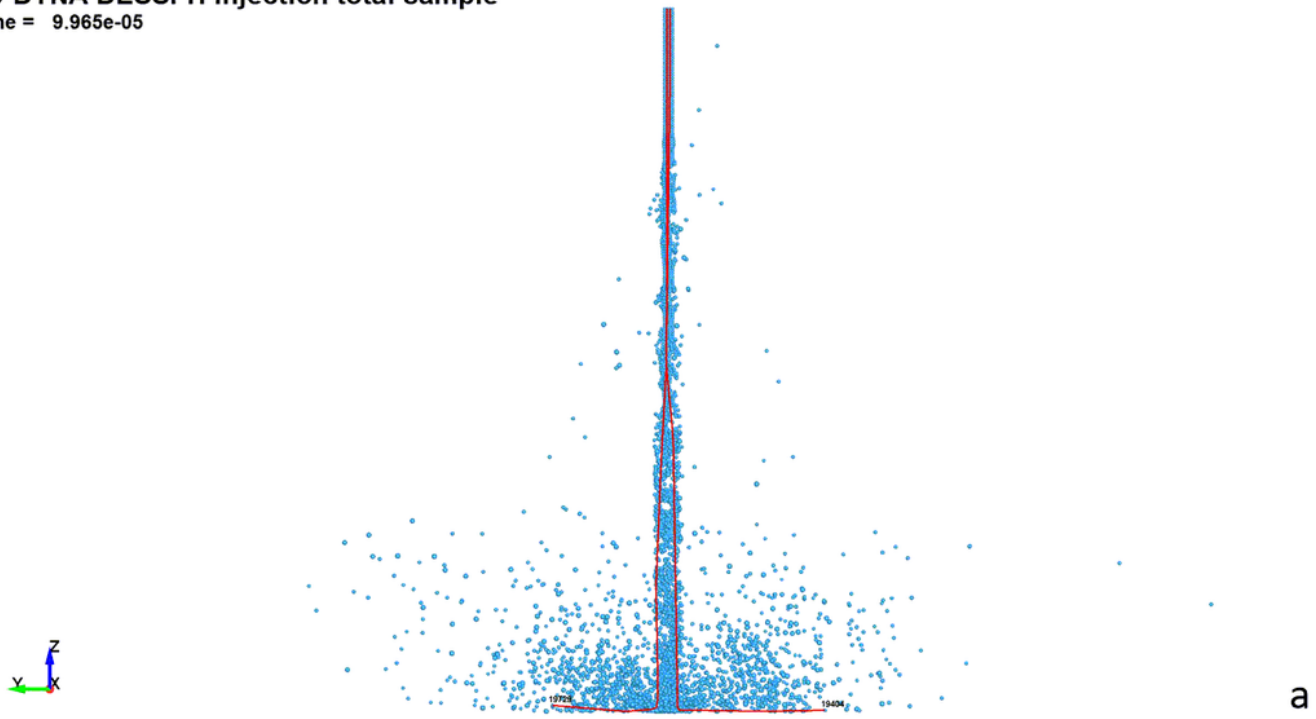


Figure 13

The detailed particle and water velocities of AWJM: (a) the evolution of abrasive particle velocities in part "a"; (b) the evolution of abrasive particle velocities in part "b"; (c) the evolution of water flow velocities.

LS-DYNA DESSPH injection total sample
Time = 9.965e-05



LS-DYNA DESSPH injection total sample
Time = 0.00030004

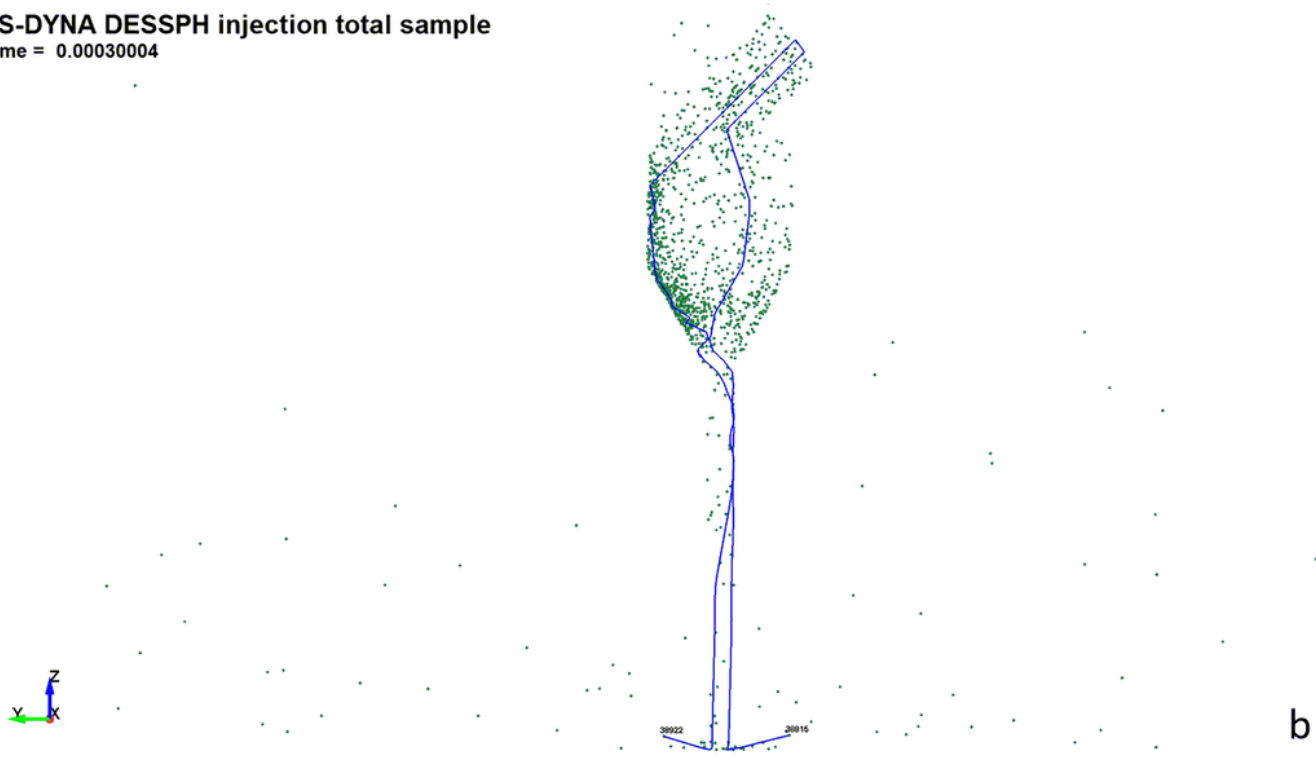
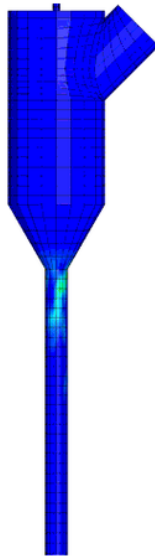


Figure 14

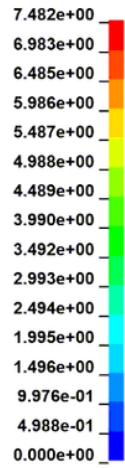
The trajectory of the water flow and abrasive particles.

LS-DYNA DESSPH injection total sample
Time = 0.000298
Contours of wear depth
min=0, at elem# 1
max=7.48214, at elem# 855



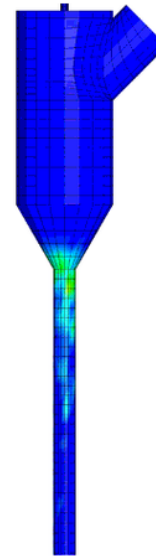
T=300µs

wear depth



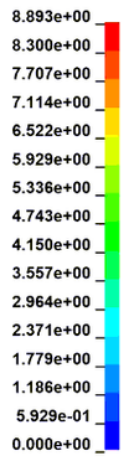
a

LS-DYNA DESSPH injection total sample
Time = 0.000398
Contours of wear depth
min=0, at elem# 1
max=8.89311, at elem# 849



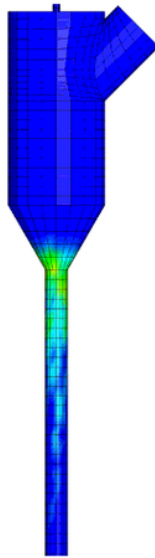
T=400µs

wear depth



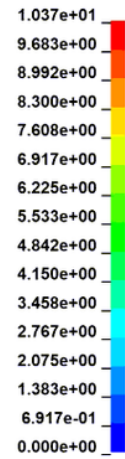
b

LS-DYNA DESSPH injection total sample
Time = 0.000498
Contours of wear depth
min=0, at elem# 1
max=10.3749, at elem# 661



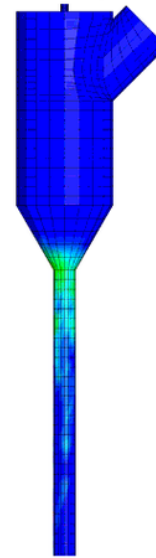
T=500µs

wear depth



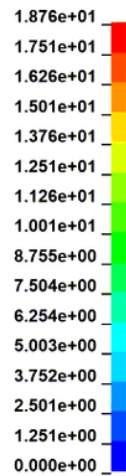
c

LS-DYNA DESSPH injection total sample
Time = 0.00059799
Contours of wear depth
min=0, at elem# 1
max=18.7607, at elem# 661



T=600µs

wear depth



d

Figure 15

The wear simulation of abrasive waterjet nozzle